An example of the use of synthetic 3.9 µm GOES-12 imagery for two-moment microphysical evaluation

Lewis D. Grasso [a] & Daniel T. Lindsey [b]

[a] Cooperative Institute for Research in the Atmosphere, Fort Collins, CO, 80523-1375, USA

[b] NOAA/NESDIS/STAR/RAMMB, Fort Collins, CO, 80523-1375, USA

PLEASE SCROLL DOWN FOR ARTICLE

Taylor & Francis
Taylor & Francis Group

An example of the use of synthetic 3.9 μm GOES-12 imagery for two-moment microphysical evaluation

LEWIS D. GRASSO*† and DANIEL T. LINDSEY‡

†Cooperative Institute for Research in the Atmosphere, Fort Collins,
CO 80523-1375, USA

‡NOAA/NESDIS/STAR/RAMMB, Fort Collins, CO 80523-1375, USA

In preparation for the launch of the next generation of geostationary satellites, considerable effort has been placed on developing new products and algorithms for operational purposes. In addition to satellite-based products and algorithms, satellite imagery can be used to evaluate numerical weather prediction models. Important first steps have already been undertaken to produce synthetic satellite imagery from numerical model output. By comparing synthetic imagery with observed imagery, model performance can be evaluated with a relatively new metric.

In this paper, synthetic Geostationary Operational Environmental Satellite (GOES)-12 imagery was used to improve the two-moment prediction of pristine ice in the RAMS (Regional Atmospheric Modeling System) mesoscale model. A thunderstorm event that occurred on 27 June 2005 over the central plains of the USA was chosen for study. Synthetic GOES-12 3.9 μm imagery of RAMS output was compared with observed GOES-12 3.9 μm imagery. A discrepancy between brightness temperatures of two anvils of thunderstorms led to an improvement in the prediction of pristine ice number concentrations. After the model was re-run, subsequent synthetic GOES-12 3.9 μm imagery of one anvil exhibited an improvement compared with observed imagery. Brightness temperatures of the second anvil became too warm, an issue that may be related to model-specified cloud condensation nuclei (CCN) concentrations. This example highlights the potential importance of using synthetic imagery to evaluate numerical weather prediction models.

1. Introduction

One method for evaluating numerical model output is to produce synthetic satellite imagery from the model fields and then compare it with observed imagery. This procedure is particularly useful when the validity of model-generated clouds and an associated microphysical scheme is examined. An early example of synthetic imagery generation from numerical model output was that of Morcrette (1991), in which output from the European Centre for Medium-Range Weather Forecasts (ECMWF) operational model was used to produce synthetic Meteosat imagery near 11.0 μm. After comparing 1 week of synthetic and observed Meteosat imagery, Morcrette (1991) concluded that clouds associated with fronts were well represented, and that synthetic brightness temperatures of high clouds were too warm. This result

---

*Corresponding author. Email: grasso@cira.colostate.edu

suggested a weakness in the way cloud coverage and cloud liquid water was diagnosed.

Chevallier and Kelly (2002) conducted a similar study over a 1-month period in December 2000. Satellite data for this study came from both Meteosat-5 and -7, and synthetic Meteosat 11.0 μm imagery was produced from the ECMWF operational model and subsequently compared with observed imagery. Results pointed to some strengths and weaknesses of the model. In particular, the location of the simulated Atlantic Intertropical Convergence Zone (ITCZ) was well represented, but simulated cirrus clouds produced by ITCZ convection were poorly represented by the model.

Synthetic Meteosat Second Generation (MSG) imagery at 8.7 and 10.8 μm was used by Chaboureau and Pinty (2006) as a means to evaluate a cirrus parameterization scheme in a numerical model. Cirrus clouds associated with tropical convection over southern Brazil in early February 2005 were the focus of this study. ECMWF data were used to initialize a regional non-hydrostatic mesoscale model, and the parameterized conversion of non-precipitating pristine ice to precipitating snow was examined. At issue was the over-depletion of pristine ice mass, the primary hydrometeor in simulated cirrus clouds, by conversion to precipitating snow. As a result of comparing synthetic to observed MSG imagery, a positive impact was noted in simulated cirrus clouds.

The work described in the present paper continues and extends the use of comparing synthetic and observed satellite imagery. Past studies typically focused on synthetic imagery near 11.0 μm and one-moment microphysical schemes (prediction of hydrometeor mass mixing ratio). In this study, synthetic imagery at 3.9 μm is used to evaluate a more complex two-moment microphysical scheme, in which both hydrometeor mass mixing ratio and number concentration are predicted. Recall that the solar and terrestrial Planck curves overlap near 3.9 μm. As a result, satellite-observed radiances at wavelength larger/smaller than 3.9 μm originate from terrestrial/solar sources. Satellite-observed radiances near 3.9 μm, however, contain not only an emitted terrestrial component, but also a reflected solar component during the daytime.

As shown by Lindsey and Grasso (2008) and Kidder *et al.* (2000), ice crystal sizes at the top of anvils of thunderstorms play a significant role in determining how much solar energy at 3.9 μm will be reflected. Past theoretical work has also demonstrated the dependence of reflectivity near 3.9 μm on the effective radius of particles. Both Nakajima and King (1990) and Wetzel *et al.* (1996) use a similar definition of the effective radius (see their equations (6) and (1), respectively) when calculating reflectance near 3.9 μm. Their results show an inverse relation between the effective radius of liquid droplets and reflectance; that is, as the effective radius decreases, reflectance near 3.9 μm increases (see figure 2 in both works).

Lindsey *et al.* (2006) reported a notable difference of brightness temperatures at 3.9 μm when comparing thunderstorms just east of the Rocky Mountains to those in the central plains. Differences in ice particle sizes within the anvils of thunderstorms can be responsible for this difference. Smaller ice particles reflect more solar energy at 3.9 μm compared with larger ice particles. As a result, data from Geostationary Operational Environmental Satellite (GOES) at 3.9 μm has been used to retrieve ice particle sizes (Lindsey and Grasso 2008). Both mass and number concentration of ice crystals must be predicted in order to accurately estimate ice crystal size, so two-moment microphysics is desirable over one-moment schemes.

As an illustration, consider the case of using one-moment prediction for cloud water. Two aspects of one-moment prediction can negatively impact accurate pristine ice size prediction. In the first case, cloud water number concentrations are fixed; if the

chosen value is too small, the resulting cloud droplets would be too large. After freezing homogeneously within the updraught, the ice crystals would also be too large, resulting in too little reflected solar energy at 3.9 μm. This may result in synthetic brightness temperatures being too low. In the second case, pristine ice number concentrations are artificially reduced or kept below a fixed value to prevent over-freezing of the cloud droplet number concentrations during the homogeneous freezing process, which would also produce ice crystals which are too large.

As part of our Geostationary Operational Environmental Satellite-R (GOES-R) risk reduction activities, the Regional Atmospheric Modeling System (RAMS; Cotton *et al.* 2003) was used to simulate convective activity that occurred on 27 June 2005 over the upper Midwest of the USA. One focus of that study was the development of an ice particle size retrieval algorithm using synthetic imagery at 2.25 μm. Data from this wavelength, currently unavailable on GOES-12, will be available from the Advanced Baseline Imager (ABI) on GOES-R (Schmit *et al.* 2005). Initially, synthetic GOES-R ABI imagery at 3.9 μm was produced and compared with observed GOES-12 imagery at 3.9 μm as a quick metric. Significant brightness temperature differences between the anvils of two thunderstorm complexes were apparent, a warning sign that there may be a problem with RAMS microphysics. This problem was subsequently identified and fixed, resulting in an improved two-moment microphysical package in RAMS.

This paper is divided into seven sections. Section 2 contains a brief description of the 27 June 2005 case study. An overview of the mesoscale model and the model that is used to produce synthetic GOES-12 3.9 μm is found in §3. Evaluation of the microphysics based on the synthetic imagery is found in §4, and §5 presents a comparison of the observed and synthetic GOES-12 3.9 μm imagery. A discussion of the differences between the synthetic and observed imagery is contained in §6 followed by the summary and conclusions in §7.

2. 27 June 2005 case study observations

On the morning of 27 June 2005, a region of high pressure moved southward from Canada into the high plains of the USA. As shown in figure 1, surface temperatures at 2000 Coordinated Universal Time (UTC) were near 30°C (85°F) over northwestern Iowa and 35°C (95°F) over southeastern Iowa. Accompanying southerly flow, surface dewpoint temperatures ranged from 21°C (70°F) to near 25°C (77°F) over that state. Over eastern Wyoming, surface temperatures were lower with values near 27°C (80°F). Typically, surface dewpoint temperatures increase after the passage of a cold front along the eastern plains of the Rocky Mountains (Doswell 1980). On this day, surface dewpoint temperatures near 13°C (55°F) extended northwestward into eastern Wyoming from western Nebraska (figure 1).

During the afternoon, thunderstorms developed over eastern Wyoming and over eastern Nebraska. In response to the mean tropospheric flow, thunderstorms over eastern Wyoming moved into western Nebraska by 2255 UTC (5:55 pm local time). During the same time period, thunderstorms also developed over eastern Nebraska and subsequently moved into Iowa (figure 2). One prominent aspect was that observed GOES-12 brightness temperatures of thunderstorm anvils at 3.9 μm were about 15–20 K lower for the thunderstorms located in Iowa compared with the thunderstorms moving out of Wyoming. This difference is also evident by the different grey shading for these thunderstorm systems.
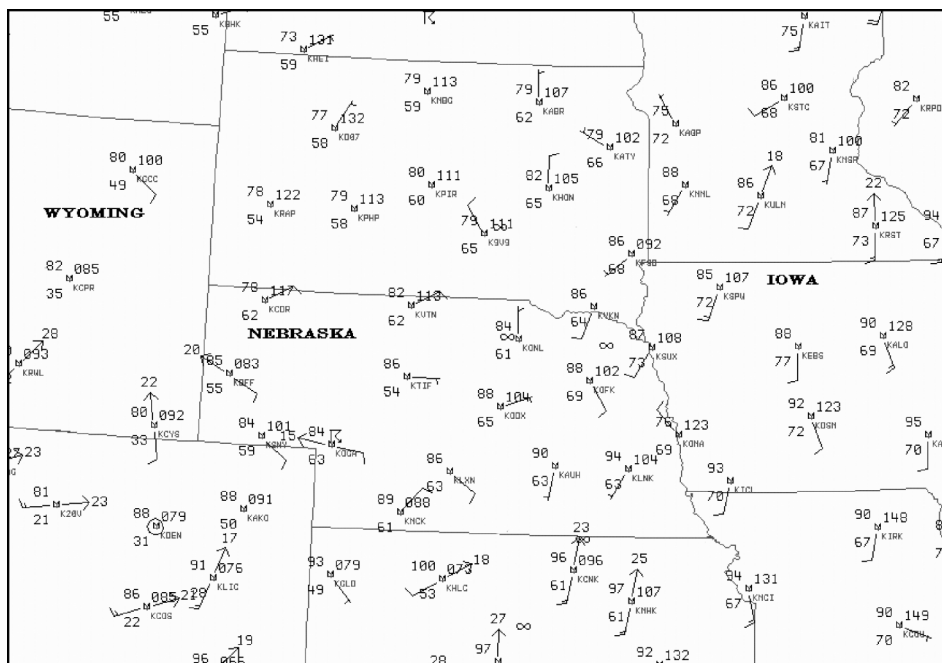
Figure 1.   Surface observations are shown for the upper Midwest from 2000 UTC 27 June 2005.
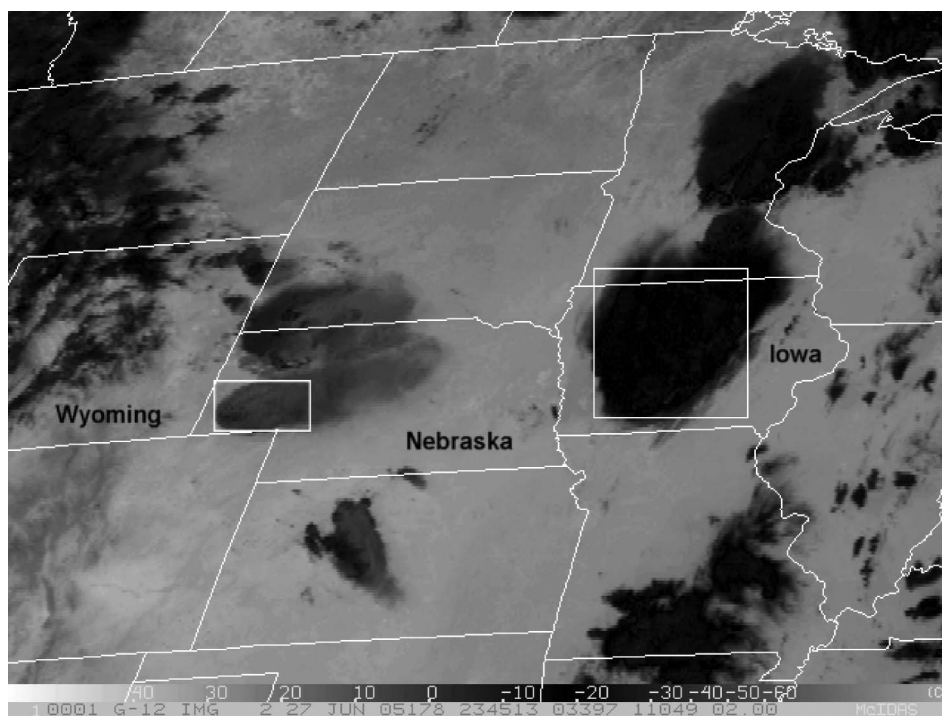

Figure 2.   Observed thunderstorms over western Nebraska and Iowa are shown in this GOES-12 3.9 μm image at 2345 UTC on 27 June 2005. White boxes indicate the region of the cloud top brightness temperatures used for histograms shown in figure 6.

3. Computational methodology

3.1 *Mesoscale model*

In order to achieve spatial and temporal variations of pristine ice mass mean diameters in conjunction with two-way communication between nested grids, RAMS (Cotton *et al.* 2003) was chosen as the mesoscale model to simulate the 27 June 2005 thunderstorm event. Due to the capability of ice clouds to reflect solar radiation at 3.9 μm, accurate prediction of pristine ice sizes was desirable. With that in mind, the version of RAMS that contains the prediction of two-moments of cloud water (Saleeby and Cotton 2004) was essential. A total of seven hydrometeor types are predicted in this version of RAMS: pristine ice, snow, aggregates, hail, graupel, rain, and two cloud water modes. Two moments are predicted for all of these hydrometeors. Definitions of these hydrometeor species are contained in Walko *et al.* (1995). As pristine ice is central to the 27 June 2005 simulation, a brief overview of this habit is justified. Pristine ice particles nucleate from vapour and grow only by vapour deposition. This habit type is confined to the smallest ice crystals ranging in size from 2 to 125 μm. Further, pristine ice is assumed to have a relatively low density, mass, and fall speed.

RAMS was initialized and nudged with the North American Regional Reanalysis (NARR) dataset (Mesinger *et al.* 2006). A 12-h simulation, beginning at 1200 UTC 27 June 2005, was conducted that contained a total of three grids for the entire simulation. Horizontal variability of soil moisture can be important for thunderstorm development (Shaw *et al.* 1997, Grasso 2000) and was therefore extracted from the NARR dataset and used to initialize soil moisture profiles in all three grids.

Three two-way interactive grids were used during the simulation. Grids 1–3 had horizontal grid spacings of 50 km, 10 km, and 2 km, respectively. A somewhat rectangular shape was necessary for grid 3 to capture the convection over eastern Wyoming and central Iowa (figure 3). All three grids had 60 vertical levels. Vertical grid spacings were 100 m near the surface, stretched by a factor of 1.1 until the spacing
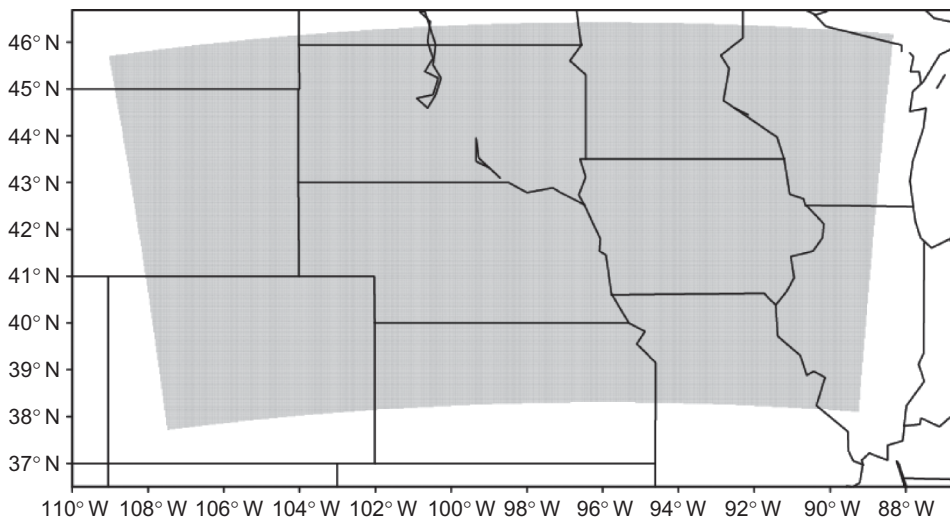

Figure 3. Shaded region depicts location of grid 3. Horizontal grid spacings in both directions were 2 km.

reached 500 m near 4.5 km. From this level to the top of the model domain, located at 24.8 km, vertical grid spacings were constant at 500 m. From 1800 UTC until the end of the simulation, model output was saved every 5 min. This output was then used to produce synthetic imagery through the use of an observational operator.

3.2 *Observational operator and synthetic imagery*

Synthetic imagery is generated from a model referred to as an observational operator. Gaseous absorption for GOES-12 at 3.9 µm was computed from the simulated pressure, temperature, and water vapour fields from RAMS. Values of the single scattering albedo, extinction, and asymmetry parameter of the seven hydrometeor types were computed from two different sources. For all hydrometeors except pristine ice, the single scattering albedo and extinction were calculated from Modified Anomalous Diffraction Theory (MADT) (Mitchell 2000). Values of the asymmetry parameter were set to 0.9 since calculated values vary little from this constant. Optical properties of pristine ice were derived using light scattering calculations that are discussed by Yang *et al*. (2000). Similar to Lindsey and Grasso (2008), a mixture of ice crystal habits was used as described by Baum *et al*. (2005). Two sources were also used to acquire values of the Legendre coefficients: first, light scattering tables were used for pristine ice; secondly, the Henyey–Greenstein formulation was used for the other six hydrometeors. Once all the optical properties are combined into bulk properties, they are passed to a one-dimensional version of the three-dimensional radiative transfer model called the Spherical Harmonic Discrete Ordinate Method (called SHDOMPP; Evans 1998). Output from SHDOMPP was the synthetic GOES-12 brightness temperatures at 3.9 µm. Additional details of the observational operator and RAMS can be found in Lindsey and Grasso (2008), Grasso *et al*. (2008), Grasso and Greenwald (2004), and Greenwald *et al*. (2002).

4. Microphysical evaluation

Synthetic GOES-12 imagery at 3.9 µm was generated from the 2-km grid. Because GOES-12 has a footprint near 4 km within the region spanned by grid 3, synthetic GOES-12 imagery was degraded to a 4 km footprint by averaging the 2 km data. Chevallier and Kelly (2002) applied a similar procedure to synthetic imagery from ECMWF output in order to best match the footprint size of observed Meteosat data. Synthetic imagery at the end of the simulation, 0000 UTC 28 June 2005, was used for comparison in this study. This time was chosen since anvils of simulated convection expanded to their largest extent. When the synthetic image (figure 4) was compared with the observed image (figure 2), brightness temperatures of the anvils of the convection over western Nebraska were about 15 K lower than observed values. This result suggested that, in general, the simulated sizes of the ice particles within the anvil were too large.

Anvils of simulated convection are composed primarily of three hydrometeor types in RAMS: aggregates, pristine ice, and snow. Grasso and Greenwald (2004) showed that the synthetic brightness temperature field of an anvil is in response to the pristine ice field. They demonstrated this by producing a synthetic image of only the pristine ice field. Their results showed good agreement, except along the edge of the pristine ice field, with an image that takes all hydrometeors into account. The reason for their result is that pristine ice self-collects to produce snow; snow and pristine ice collect to produce aggregates. Due to differential sedimentation, snow and aggregates sink
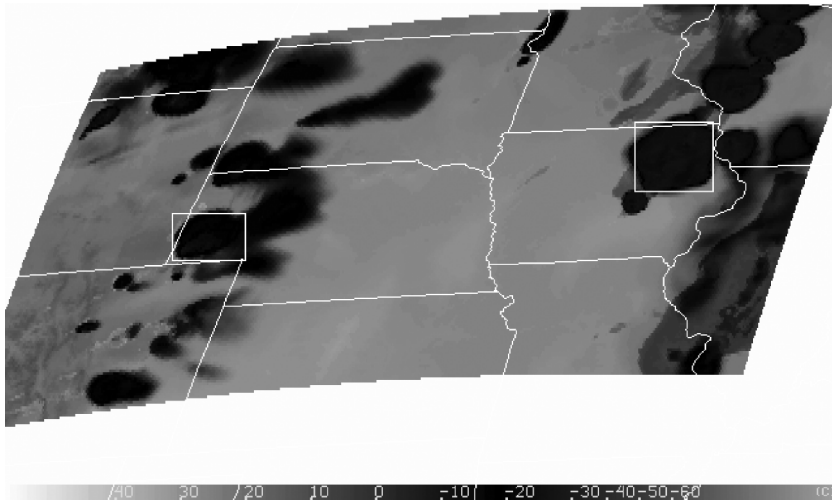
Figure 4. Simulated thunderstorms over western Nebraska and Iowa are shown in this synthetic GOES-12 3.9 μm image at 0000 UTC on 28 June 2005. White boxes indicate the region of the cloud top brightness temperatures used for histograms in figure 6.

leaving pristine ice at the top of a simulated anvil. As a consequence of their work, the calculation of the two-moments of pristine ice, in RAMS, was evaluated for the simulation of the 27 June 2005 event.

Three sources of pristine ice in the anvil of a simulated thunderstorm can be identified in RAMS: homogeneous freezing of haze, heterogeneous nucleation of ice nuclei, and homogeneous freezing of cloud water (Walko *et al.* 1995, Meyers *et al.* 1997, Saleeby and Cotton 2004). As part of the current work, sensitivity testing demonstrated that both the homogeneous freezing of haze and heterogeneous nucleation of ice nuclei are unable to account for the mass mixing ratio and/or the number concentration of the pristine ice field in the anvil of a simulated thunderstorm. Therefore, the process of homogeneous freezing of cloud droplets was examined.

In RAMS, cloud droplets develop from condensation of water vapour onto a prescribed population of aerosol particles. As the cloud droplets ascend within the updraught of a simulated storm, they eventually reach and pass through the homogeneous freezing layer. After passing through this layer, cloud droplet mass and number concentrations are converted into pristine ice mass and number concentrations. Thus, a somewhat continuous pattern of the sum of cloud water mass and pristine ice mass should be evident in a vertical cross-section through an updraught that contains the homogeneous freezing layer. Similar remarks hold for the sum of cloud water number concentrations and pristine ice number concentrations. While this was true for the sum of cloud water mass and pristine ice mass in the present study, a notable decrease occurred in cloud water number concentrations to pristine ice number concentrations. This suggested an artificial loss of pristine ice number concentrations and consequently the existence of relatively large pristine ice particles. This is consistent with the brightness temperatures of the anvil of the simulated storm in western Nebraska being too low compared to observations.

In all of the previous versions of RAMS, only one moment of cloud water was predicted: cloud water mass. Cloud water number concentrations were specified and
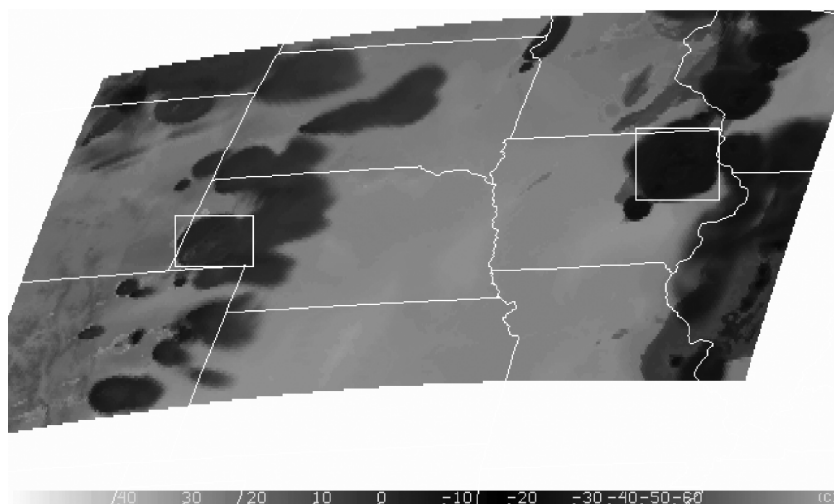
Figure 5. This synthetic image is the same as figure 4, but for the new simulation.

held constant during a simulation of a thunderstorm. As a result, the over production of pristine ice number concentrations from homogeneous freezing of cloud water could be problematic. In order to circumvent this problem, pristine ice number concentrations were artificially reduced at each time step. This process was done in the homogeneous freezing layer to prevent the over production of pristine ice number concentrations.

In the version of RAMS used for this study, two moments of cloud water are predicted: mass mixing ratio and number concentration. Thus, the artificial reduction of pristine ice number concentrations should have been removed. However, such a reduction was still present. Sensitivity tests were subsequently conducted in which the artificial reduction of pristine ice number concentrations was removed. Results from these tests showed the expected somewhat continuous pattern of the sum of cloud water number concentrations and pristine ice number concentrations in vertical cross-sections. Subsequently, the simulation of the 27 June 2005 convective event was re-run and a new synthetic GOES-12 image at 3.9 μm was produced (figure 5). A comparison of brightness temperatures of the anvil of the thunderstorm over western Nebraska (figures 4 and 5) shows a noticeable increase in brightness temperatures in the new run.

5. Synthetic and observed GOES-12 3.9 μm imagery

A comparison between the observed and synthetic GOES-12 imagery at 3.9 μm can be made through the use of histograms. Brightness temperatures are plotted in histograms for the observed and synthetic data from both the old run and new runs (figure 6). Consider the thunderstorm over western Nebraska in the observed and synthetic imagery. A box has been placed over the anvil of the storm and is displayed in figures 2, 4 and 5. Brightness temperatures of that portion of the anvil contained in the box are plotted in the histogram in figure 6(*a*). As can be seen, the original simulation produced an anvil with brightness temperatures that were about 15 K lower (black columns) than those of the observed anvil (light grey columns). This was a result of the
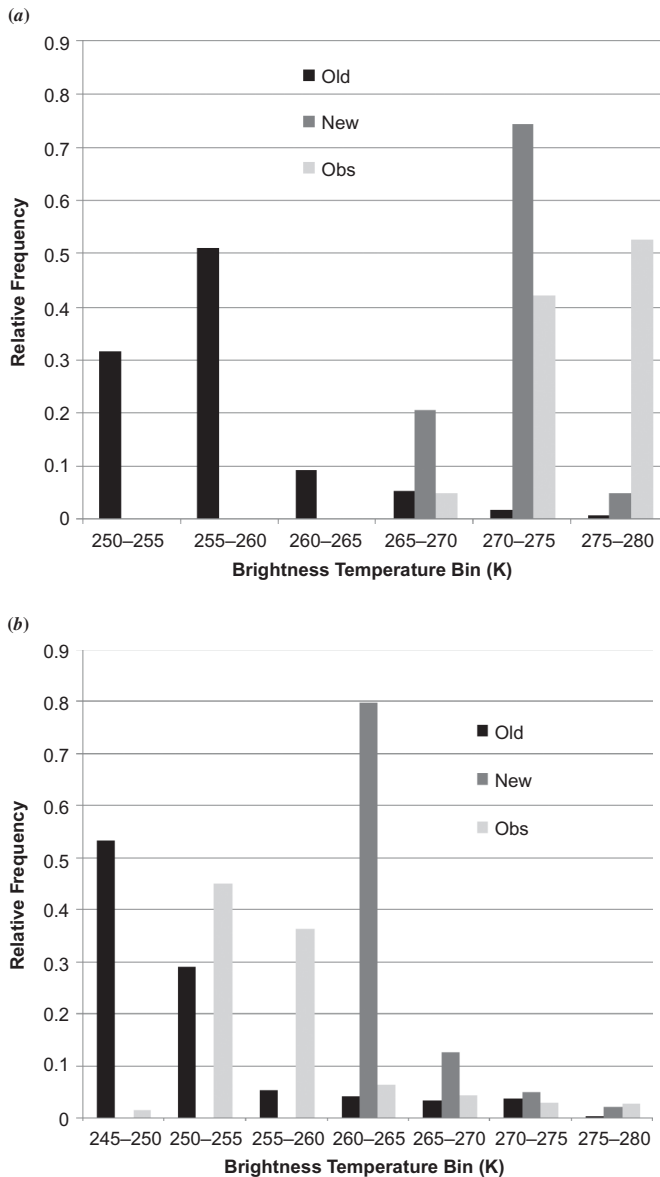
(a)

(b)

Figure 6. Two histograms depict brightness temperatures from three different sources: observed GOES-12 data (Obs); synthetic GOES-12 data from the original simulation (Old); and synthetic GOES-12 data from the new simulation (New). The histogram in (a) is for the thunderstorm over western Nebraska while the histogram in (b) is for the thunderstorm over Iowa.

simulation producing pristine ice particles that were too large. As a result, less solar energy at 3.9 μm was reflected back to space. In the new run, however, the simulation produced smaller pristine ice particles. As a consequence, more solar energy at 3.9 μm was reflected back to space. This gave rise to synthetic brightness temperatures (grey columns) that were not only larger than those of the old run, but also similar to observed brightness temperatures. The thunderstorms over Iowa were examined next.

As a result of the colour table used to display brightness temperatures in figures 2, 4 and 5, discrepancies of brightness temperatures of the anvil in Iowa were less obvious. A histogram, similar to figure 6(*a*), was produced for this storm and is shown in figure 6(*b*). A box was also placed over the anvil of the thunderstorm over Iowa in figures 2, 4 and 5. Brightness temperatures of the anvils within the box were used to build the histogram shown in figure 6(*b*). Similar to the results of the storm over western Nebraska, the old run produced brightness temperatures (black columns) that were lower compared with those of the observed thunderstorm (light grey columns). However, the difference between brightness temperatures of the old run and observations for this storm were not as large as those of the thunderstorm over western Nebraska. Unlike the results of the storm over western Nebraska, the new run produced brightness temperatures (grey columns) that were larger than those of the observed thunderstorm. In fact, synthetic brightness temperatures of the anvil of the thunderstorm over Iowa in the new run are too high. In other words, the new run produced synthetic brightness temperatures that compare reasonably well with observations for the storm over western Nebraska, while those of the Iowa storm are too high.

Synthetic GOES-12 imagery at 10.7 μm was also compared with observed GOES-12 imagery at 10.7 μm. As seen in figure 7, synthetic brightness temperatures from the original run compare favourably with observations. A comparison between the histogram in figure 6(*a*) with the histogram in figure 7(*c*) indicates that the relatively large discrepancy between synthetic and observed brightness temperatures at 3.9 μm for the thunderstorm over western Nebraska in the original run was absent at 10.7 μm.

6. Discussion

Comparing synthetic imagery of the simulated thunderstorms to observed imagery of thunderstorms led to a necessary modification of the two-moment prediction of pristine ice in RAMS. On the one hand, this improvement led to beneficial results for the simulated thunderstorm over western Nebraska. On the other hand, this improvement led to a lack of beneficial results for the simulated thunderstorm over Iowa. This dilemma centres on one challenging aspect of simulating thunderstorms: simulating anvils that, in one case, have small enough ice particles to reflect relatively large amounts of solar energy at 3.9 μm; and simulating anvils that, in the other case, have large enough ice particles to reflect relatively small amounts of solar energy at the same wavelength in the same simulation. In fact, this is why the 27 June 2005 event is ideal for this type of study. The comparison of synthetic imagery from the new run with observed imagery still suggests an area of improvement in RAMS. That is, what is needed to maintain the brightness temperatures of the anvil of the thunderstorm over western Nebraska and at the same time reduce the brightness temperatures of the anvil of the thunderstorm over Iowa?

As stated above, older versions of RAMS required the specification of cloud droplet number concentrations. In the version used in this study, cloud droplet number concentrations are predicted. In addition, cloud droplets develop from a specified population of aerosol particles that serve as cloud condensation nuclei (CCN). Once specified, they are initialized in a horizontally homogeneous manner. Although initializing CCN in a horizontally homogeneous manner may be a good first step, observed CCN profiles are likely to contain significant horizontal variability. One possible way to reduce the synthetic GOES-12 3.9 μm brightness temperatures of the anvil of the thunderstorm over Iowa is through the use of horizontally
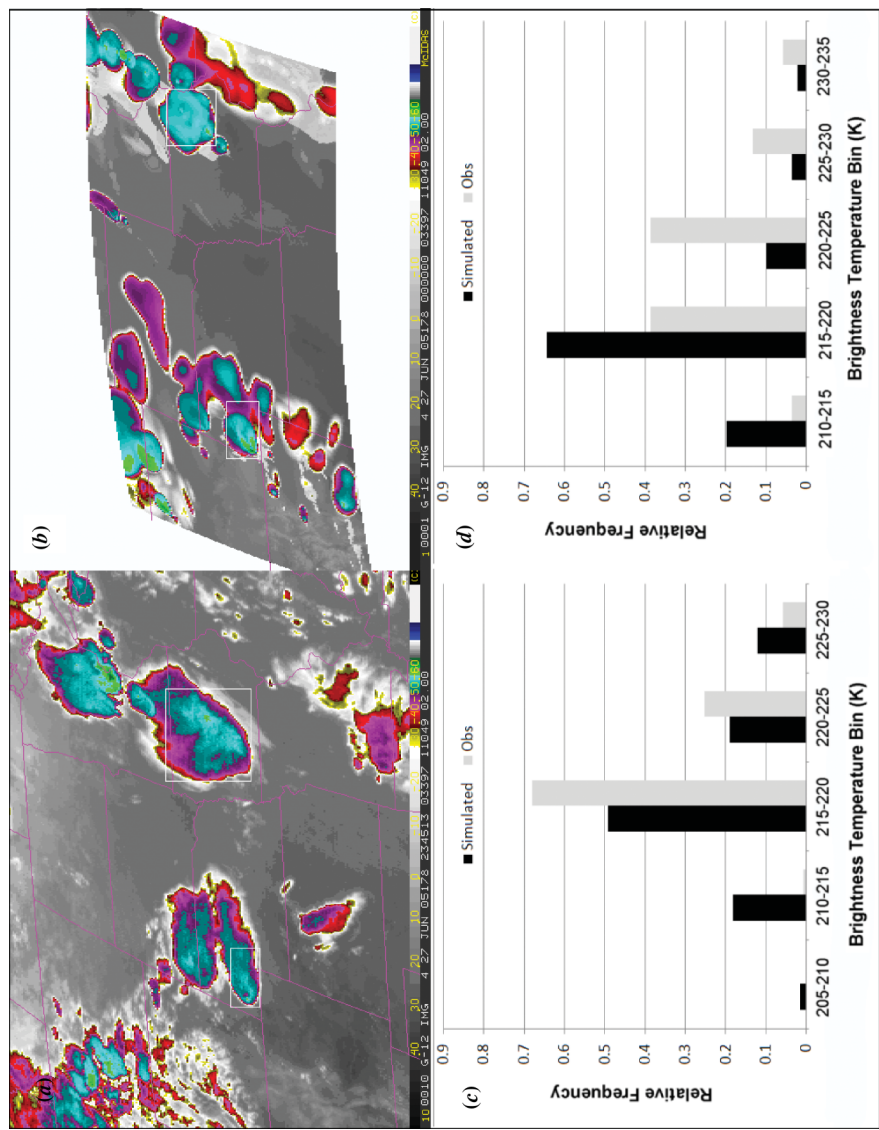
Figure 7. (a) Observed GOES-12 image, as in figure 2, but at 10.7 µm, (b) synthetic GOES-12 image from the original run, as in figure 4, but at 10.7 µm. Histograms of observed and synthetic GOES-12 brightness temperatures at 10.7 µm for the thunderstorm over (c) western Nebraska and (d) Iowa.

variable CCN concentrations. Lower values of CCN over Iowa would lead to larger cloud droplets and thus larger pristine ice particles.

Climatological studies have shown that, in general, anvils of thunderstorms near the Rockies reflect more solar energy at 3.9 μm compared to storms towards the east (Lindsey *et al*. 2006). They used reanalysis data to show that anvils of thunderstorms that reflect more solar energy at 3.9 μm exist in environments that have larger values of vertical shear, boundary layers with lower water vapour mixing ratios, and steeper lower to middle troposphere environmental lapse rates. In addition, reanalysis data also supported that the distance between cloud base and the homogeneous freezing level was smaller for anvils that reflected more solar energy at 3.9 μm. This last feature could be related to the higher terrain values near the Rockies. Current work is exploring the role of CCN number concentrations as part of an explanation for the different reflectivities of thunderstorm anvils put forth by Lindsey *et al*. (2006). Results from this work could highlight the importance of geographic variability of CCN number concentrations on the radiative properties of anvils.

Understanding the role of aerosols in cloud microphysics may lead to a significant development in the area of numerical modelling and observations. This would require the identification of aerosols, their chemical composition, source, and if they serve as CCN or ice nuclei. New routines could be added into numerical models to simulate the movement of aerosols and their interaction with cloud microphysics. In order for numerical models to be initialized with variable aerosol concentrations, an observing network of sufficient resolution would be needed. Similar ideas concerning the impact of aerosols on cloud microphysics has also been discussed by Wang *et al*. (2009).

7.   Summary and conclusions

Synthetic satellite data from numerical model output has been used in past research for model validation. This was done by comparing synthetic imagery from model output with observed imagery near 11.0 μm for a given satellite. This study extended past work by producing synthetic imagery at 3.9 μm of a convective event. Imagery at 3.9 μm differs from imagery near 11.0 μm due to the added reflective solar component at the smaller wavelength.

One goal of this work was to develop a retrieval algorithm for ice particle sizes in the anvils of thunderstorms. Preliminary results exhibited a significant departure of synthetic GOES-12 brightness temperatures of anvils of simulated convection compared to observed GOES-12 imagery at 3.9 μm in the range of 5–15 K. Brightness temperatures were too low, suggesting that ice particles in the simulated anvil were too large. This departure led to the improvement of the two-moment prediction of pristine ice, the dominant radiatively active hydrometeor in the anvils of simulated convection.

Once the model was re-run, synthetic brightness temperatures of the anvils of the two main simulated thunderstorms changed. Brightness temperatures of the anvil of the thunderstorm located in western Nebraska increased to near observed values. In contrast, brightness temperatures of the anvil of the thunderstorm over Iowa increased too much, exceeding observed values. This result suggested that RAMS was unable to produce one anvil with relatively small ice particles and, at the same time, produce another anvil with relatively large ice particles. A possible cause may be the horizontally constant profile of specified CCN number concentrations.

One significant outcome of this work is demonstrating the potential use of synthetic imagery of model output. Synthetic GOES-12 3.9 μm imagery, when compared to observed GOES-12 3.9 μm imagery, suggested two areas in RAMS that needed improvement. One area is the prediction of two-moments of pristine ice while the other is the potential need for horizontally variable CCN number concentrations. In conclusion, synthetic satellite data has been shown to be an important and potentially valuable tool for model evaluation.

References

BAUM, B.A., HEYMSFIELD, A.J., YANG, P. and BEDKA, S.T., 2005, Bulk scattering properties for the remote sensing of ice clouds. Part I: Microphysical data and models. *Journal of Applied Meteorology*, **44**, pp. 1885–1895.

CHABOUREAU, J.-P. and PINTY, J.-P., 2006, Evaluation of a cirrus parameterization with Meteosat Second Generation. *Geophysical Research Letters*, **33**, L03815, doi: 10.1029/ 2005GL024725.

CHEVALLIER, F. and KELLY, G., 2002, Model clouds as seen from space: comparison with geostationary imagery in the 11-μm window channel. *Monthly Weather Review*, **130**, pp. 712–722.

COTTON, W.R., PIELKE, SR, R.A., WALKO, R.L., LISTON, G.E., TREMBACK, C.J., JIANG, H., MCANELLY, R.L. HARRINGTON, J.Y., NICHOLLS, M.E., CARRIO, G.G. and MCFADDEN, J.P., 2003, RAMS 2001: current status and future direction. *Meteorology and Atmospheric Physics*, **82**, pp. 5–29.

DOSWELL III, C.A., 1980, Synoptic-scale environments associated with high plains severe thunderstorms. *Bulletin of the American Meteorological Society*, **61**, pp. 1388–1400.

EVANS, K.F., 1998, The spherical harmonics discrete ordinate method for three-dimensional atmospheric radiation transfer. *Journal of Atmospheric Science*, **55**, pp. 429–446.

GRASSO, L.D., SENGUPTA, M., DOSTALEK, J.F., BRUMMER, R. and DEMARIA, M. 2008, Synthetic satellite imagery for current and future environmental satellites. *International Journal of Remote Sensing*, **29**, pp. 4373–4384.

GRASSO, L.D. and GREENWALD, T., 2004, Analysis of 10.7 μm brightness temperatures of a simulated thunderstorm with two-moment microphysics. *Monthly Weather Review*, **132**, pp. 815–825.

GRASSO, L.D., 2000, A numerical simulation of dryline sensitivity to soil moisture. *Monthly Weather Review*, **128**, pp. 2816–2834.

GREENWALD, T.J., HERTENSTEIN, R. and VUKICEVIC, T., 2002, An all-weather observational operator for radiance data assimilation with mesoscale forecast models. *Monthly Weather Review*, **130**, pp. 1882–1897.

KIDDER, S.Q., HILLGER, D.W., MOSTEK, A.J. and SCHRAB, K.J., 2000, Two simple GOES Imager products for improved weather analysis and forecasting. *National Weather Digest*, **24**, pp. 25–30.

LINDSEY, D.T., HILLGER, D.W., GRASSO, L., KNAFF, J.A. and DOSTALEK, J.F., 2006, GOES climatology and analysis of thunderstorms with enhanced 3.9 μm reflectivity. *Monthly Weather Review*, **134**, pp. 2342–2353.

LINDSEY, D.T. and GRASSO, L., 2008, An effective radius retrieval for thick ice clouds using GOES. *Journal of Applied Meteorology and Climatology*, **47**, pp. 1222–1231.

MESINGER, F., DIMEGO, G., KALNAY, E., MITCHELL, K., SHAFRAN, P.C., EBISUZAKI, W., JOVIC, D., WOOLEN, J., ROGERS, E., BERBERY, E.H., EK, M.B., FAN, Y., GRUHPAINE, R., HIGGINS, W., LI, H., LIN, Y., MANIKIN, G., PARRISH, D. and SHI, W., 2006, North American regional reanalysis. *Bulletin of American Meteorological Society*, **87**, pp. 343–360.

MEYERS, M.P., WALKO, R.L., HARRINGTON, J.Y. and COTTON, W.R., 1997, New RAMS cloud microphysics parameterization. Part II: the two-moment scheme. *Atmospheric Research*, **45**, pp. 3–39.

MITCHELL, D.L., 2000, Parameterization of the Mie extinction and absorption coefficients for water clouds. *Journal of Atmospheric Science*, **57**, pp. 1311–1326.

MORCRETTE, J.-J, 1991, Evaluation of model-generated cloudiness: satellite-observed and model-generated diurnal variability of brightness temperatures. *Monthly Weather Review*, **119**, pp. 1205–1224.

NAKAJIMA, T. and KING, M.D., 1990, Determination of the optical thickness and effective particle radius of clouds from reflected solar radiation measurements. Part I: Theory. *Journal of Atmospheric Science*, **47**, pp. 1878–1893.

SALEEBY, S.M. and COTTON, W.R., 2004, A large-droplet mode and prognostic number concentration of cloud droplets in the Colorado State University Regional Atmospheric Modeling System (RAMS). Part I: module descriptions and supercell test simulations. *Journal of Applied Meteorology*, **43**, pp. 182–195.

SCHMIT, T.J., GUNSHOR, M.M., PAUL, W. MENZEL, J. LI, BACHMEIER, S. and GURKA, J., 2005, Introducing the next-generation advanced baseline imager (ABI) on Geostationary Operational Environmental Satellites (GOES)-R. *Bulletin of the American Meteorological Society*, **86**, pp. 1079–1096.

SHAW, B.L., PIELKE, R.A. and ZIEGLER, C.L., 1997, The effect of soil moisture heterogeneity on a Great Plains dry line: a numerical study. *Monthly Weather Review*, **125**, pp. 1489–1506.

WALKO, R., COTTON, W.R., MEYERS, M.P. and HARRINGTON, J.Y., 1995, New RAMS cloud microphysics parameterization. Part I: the single-moment scheme. *Atmospheric Research*, **38**, pp. 29–62.

WANG, J., VAN DEN HEEVER, S.C. and REID, J.S., 2009, A conceptual model for the link between Central American biomass burning aerosols and severe weather over the south central United States. *Environmental Research Letters*, **4**, doi: 10.1088/1748.9326/4/1/015003.

WETZEL, M.A., BORYS, R.D. and XU, L.E., 1996, Satellite microphysical retrievals for land-based fog with validation by balloon profiling. *Journal of Applied Meteorology*, **35**, pp. 810–829.

YANG, P., LIOU, K.N., WYSER, K. and MITCHELL, D., 2000, Parameterization of the scattering and absorption properties of individual ice crystals. *Journal of Geophysical Research*, **105**, pp. 4699–4718.